Inorg. Chem. **2008**, *47*, 121–127

Solventless Nanoparticles Synthesis under Low Pressure

Hyun Gil Cha,[†] Don Keun Lee,[‡] Young Hwan Kim,[†] Chang Woo Kim,[†] Chung Sup Lee,[§] and Young Soo Kang*,[†]

Department of Chemistry, Pukyong National University, Namgu, Busan 608-737, South Korea, Cheil Industries Inc., Gocheon-Dong, Uiwang-Si, Gyeonggi-Do 437-711, South Korea, and Department of Physics, Pukyong National University, Namgu, Busan 608-737, South Korea

Received August 7, 2007

In the present study, metal nanocrystals were obtained by the very easy, economical, and nontoxic thermal decomposition method and stabilized by coating oleate without any solvent. These nanocrystals have a highly crystalline structure due to a high decomposition temperature (∼563–573 K) at low pressure and very narrow distribution. The prepared Fe_3O_4 nanocrystals were controlled by the annealing time and vacuum pressure. A TEM image of monodispersed Fe_3O_4 nanocrystals showed the 2D assembly of nanocrystals, demonstrating their uniformity. The particle size is 10.6 ± 1.2 nm. TEM images of silver nanocrystals a showed 2D assembly with 9.5 ± 0.7 nm. An electron diffraction image and X-ray diffraction of the nanocrystals showed the highly crystalline nature of metal nanocrystals.

Introduction

The synthesis of monodispersed nanocrystals is of key importance because the properties of these nanocrystals depend strongly on their dimensions. For example, the color sharpness of semiconductor nanocrystal-based optical devices is strongly dependent on the uniformity of the nanocrystals,[1−4] and monodisperse magnetic nanocrystals are critical for the next-generation multi-terabit magnetic storage media.[5−7] For these monodisperse nanocrystals to be used, an economical mass-production method needs to be developed. Unfortunately, in most syntheses reported so far, only sub-gram quantities of monodisperse nanocrystals were produced. Uniform-sized nanocrystals of CdSe[8,9] and gold[10,11] have been produced using colloidal chemical synthetic procedures. In addition, monodispersed magnetic nanocrystals such as iron,[12] cobalt,[13] α-Fe_2O_3,[14] and Fe_3O_4[15,16] have been synthesized using various synthetic methods.[17] As these syntheses are generally carried out in solution and it is impossible in practice to completely eliminate coagulation. Korgel et al. have pioneered the synthesis of nanoparticles in the absence of solvent.[18−21] Scheme 1 shows a schematic drawing of the nontoxic synthesis of functional nanoparticles without any solvent. The metal−oleate complex serves as the molecular precursor and provides the capping ligand to control particle growth. In the solventless reaction environment, interparticle collisions rarely occur, and particle growth proceeds prima-

* To whom correspondence should be addressed. E-mail: yskang@pknu.ac.kr.
[†] Department of Chemistry, Pukyong National University.
[‡] Cheil Industries Inc.
[§] Department of Physics, Pukyong National University.

(1) Alivisatos, A. P. *Science* **1996**, *271*, 933.
(2) Nirmal, M.; Brus, L. *Acc. Chem. Res.* **1999**, *32*, 407.
(3) Murray, C. B.; Kagan, C. R.; Bawendi, M. G. *Annu. Rev. Mater. Sci.* **2000**, *30*, 545.
(4) Rogach, A. L.; Talapin, D. V.; Shevchenko, E. V.; Kornowski, A.; Weller, H. *Adv. Funct. Mater.* **2002**, *12*, 653.
(5) Sun, S.; Murray, C. B.; Weller, D.; Folks, L.; Moser, A. *Science* **2000**, *287*, 1989.
(6) Speliotis, D. E. *J. Magn. Magn. Mater.* **1999**, *193*, 29.
(7) O'Handley, R. C. In *Modern Magnetic Materials*; Wiley & Sons: New York, 1999.
(8) Murray, C. B.; Norris, D. J.; Bawendi, M. G. *J. Am. Chem. Soc.* **1993**, *115*, 8706.
(9) Peng, X.; Wickham, J.; Alivisatos, A. P. *J. Am. Chem. Soc.* **1998**, *120*, 5343.
(10) Kim, F.; Song, J.; Yang, P. *J. Am. Chem. Soc.* **2002**, *124*, 14316.
(11) Jana, N. R.; Peng, X. *J. Am. Chem. Soc.* **2003**, *125*, 14280.
(12) Dumestre, F.; Chaudret, B. *Science* **2004**, *303*, 821.
(13) Puntes, V. F.; Krishnan, K. M.; Alivisatos, A. P. *Science* **2001**, *291*, 115.
(14) Hyeon, T.; Lee, S. S.; Park, J.; Chung, Y.; Na, H. B. *J. Am. Chem. Soc.* **2001**, *123*, 12798.
(15) Pileni, M. P. *Nat. Mater.* **2003**, *2*, 145.
(16) Sun, S.; Zeng, H.; Robinson, D. B.; Raoux, S.; Rice, P. M.; Wang, S. X.; Li, G. *J. Am. Chem. Soc.* **2004**, *126*, 273.
(17) Neveu, P. S.; Cabuil, V.; Massart, R.; Escaffe, R.; Dussaud, J. *J. Magn. Magn. Mater.* **1993**, *122*, 42.
(18) Sigman, M. B.; Korgel, B. A. *Chem. Mater.* **2005**, *17*, 1655.
(19) Larsen, T. H.; Sigman, M.; Ghezelbash, A.; Doty, C.; Korgel, B. A. *J. Am. Chem. Soc.* **2003**, *125*, 5638.
(20) Ghezelbash, A.; Sigman, M. B.; Korgel, B. A. *Nano Lett.* **2004**, *4*, 537.
(21) Sigman, M. B.; Ghezelbash, A.; Hanrath, T.; Saunders, A. E.; Lee, F.; Korgel, B. A. *J. Am. Chem. Soc.* **2003**, *125*, 16050.

10.1021/ic701570z CCC: $40.75
Published on Web 12/07/2007

Scheme 1. Procedure of the Synthesis of Nanocrystallites Using M−oleate Complex (M = Ag^+, Fe^{2+}, etc.)[a]

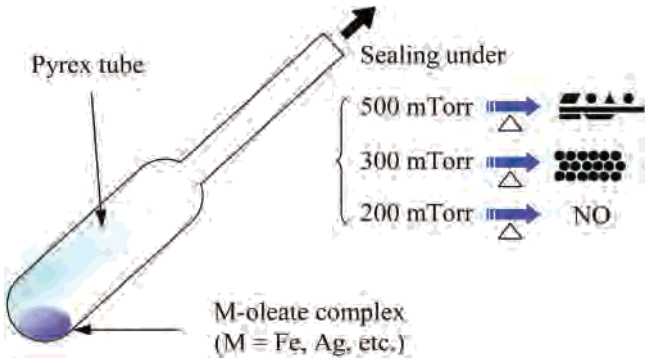

[a] The precursors were prepared from the reaction of metal chlorides and sodium oleate in water. The thermalysis of the complex was performed under low pressure at about 593 K without any solvent.

rily by monomer addition to the particle surface, leading to monodispersed size and shape distributions.[22] The advantages of this method is that one does not need to make a separation nor to evaporate solvent.

2. Experimental Section

2.1. Materials. $FeCl_2 \cdot 4H_2O$ (99+%), $AgNO_3$ (99+%), and sodium oleate ($C_{17}H_{33}COONa$, 98%) were used as supplied from Sigma-Aldrich. Hexanes was purchased from Jusei Co and used as received. Water was doubly distilled and deionized.

2.2. Synthesis of Fe_3O_4 Nanocrystals. To prepare iron−oleate complex, 2 g of $FeCl_2 \cdot 4H_2O$ (10 mmol) was dissolved in deoxygenated water, and the resulting solution was added into 6.09 g of sodium oleate (20 mmol) under vigorous stirring for 2 h. The precipitate was separated by filtration and washed with doubly deionized water to be free of sodium and chlorine ions. After drying, the Fe^{+2}−$oleate_2$ complex was transferred into the pyrex tube. The complex was first flushed with nitrogen, and the tube was sealed under 300 mTorr. The sample was slowly heated from room temperature to 593 K at 1 K/min. After reaching the desired temperature, it was held at 593 K for 2 h and cooled to room temperature. The complex color was changed to black, indicating that Fe_3O_4 nanoparticles were being formed. The iron oxide nanocrystals can be easily redispersed in hexane.

2.3. Synthesis of Silver Nanocrystals. To prepare the Ag^{+1}−oleate complex, 1.7 g of $AgNO_3$ (10 mmol) was dissolved in deoxygenated water (300 mL, 18 MΩ, nitrogen gas bubbling for 30 min), and the resulting solution was added into 3.05 g of sodium oleate (10 mmol) under vigorous stirring for 2 h. The precipitate was separated by filtration and washed with doubly deionized water to be free of sodium and nitrate ions. After drying, the Ag^{+1}−oleate complex was transferred into the pyrex tube. The complex was first flushed with nitrogen, and the tube was sealed at 300 mTorr. The sample was slowly heated from room temperature to 563 K by 2 K/min, and it was annealed at 563 K for 1 h and cooled to room temperature. The complex color was changed to black, indicating that silver nanocrystals were being formed. The silver nanocrystals can be easily redispersed in hexane.

2.4. Characterization. To identify the structure and properties of the synthesized metal nanoparticles, we performed various experiments. The crystal structure of the synthesized nanocrystals was identified by X-ray powder diffraction (XRD) with a Philips X'Pert-MPD System with a Cu Kα radiation source ($\lambda = 0.154056$ nm). The size and shape of the nanoparticles were obtained by transmission electron microscopy (TEM). TEM measurements were carried out on Hitachi H-7500 (low-resolution) and a JEOL JEM2010 (high-resolution) transmission electron microscopes. Samples for TEM study were prepared on 300 mesh copper grids coated with carbon. A drop of metal nanocrystal solution was carefully placed on the copper grid surface and dried. The size distributions of the nanocrystals were measured from enlarged photographs of the TEM images. The magnetization curve of Fe_3O_4 nanocrystals was characterized with the Lake Shore 7300 vibrating sample magnetometer (VSM). Mössbauer spectra were recorded using a conventional Mössbauer spectrometer of the electromechanical type with a 20 mCi ^{57}Co source in a rhodium matrix. To produce uniform thickness over the area of the Mössbauer absorber, a sample was mixed with boron nitride powder. The area density of iron for the flattened sample was 10 mg/cm^2. The size distribution and characterization of the nanocomposite film of the surface coated Fe_3O_4 nanocrystals was done with TEM analysis. The optical property of the silver nanoparticles has been characterized by absorption spectroscopy. UV−vis absorption spectra of the synthesized silver nanocrystals were taken using a Varian, Cary 1C. Thermal analysis was performed under vacuum conditions with a heating rate of 10 K/min using a PerkinElmer TGA 7 connected with a vacuum system.

3. Results and Discussions

To synthesize monodispersed metal nanoparticles, we modified the published procedure[23] using thermal decomposition of the metal−oleate complex in the absence of surfactants and solvent. When pure metal carboxylates are heated, the organic moiety in the metal−oleate complex was decomposed at temperatures near to or higher than 300 °C. The thermal decomposition reaction of transition metal carboxylates occurs via the formation of thermal free radicals, as shown in previous work.[24] As the temperature increases, the breakage of M−O and MO−C bonds in metal carboxylate results in radical species according to eqs 1 and 2.

$$M{-}OOCR \rightarrow M^* + {}^*OOCR \quad (1)$$

$$M{-}OOCR \rightarrow MO^* + OC^*R \quad (2)$$

From the reaction between the simultaneously formed radical species, these species can combine, decompose into smaller molecules, or react with other metal carboxylate molecules to propagate to decompose metal carboxylates in the metal−oleate complex. We controlled the morphologies of metal nanoparticles by temperature and vacuum pressure. As Fe_3O_4 nanocrystals were studied as a model for different morphologies of metal nanoparticles by thermal decomposition, we observed that the morphology of metal nanoparticles depends on the annealing time and vacuum pressure.

3.1. Fe_3O_4 Nanocrystals. Part A of Figure 1 is a low-resolution TEM image of monodisperse Fe_3O_4 nanocrystallites. All of the Fe_3O_4 particles are spherical. The mean size of the Fe_3O_4 nanoparticles is 10.6 nm, with a standard deviation of 1.2 nm, which was obtained from enlarged

(22) Teranishi, T.; Hasegawa, S.; Shimizu, T.; Miyke, M. *Adv. Mater.* **2001**, *13*, 1699.
(23) Han, Y. C.; Cha, H. G.; Kim, C. W.; Kim, Y. H.; Kang, Y. S. *J. Phys. Chem. C* **2007**, *111*, 6275.
(24) Kenfack, F.; Langbein, H. *Thrermochim. Acta* **2005**, *426*, 61.

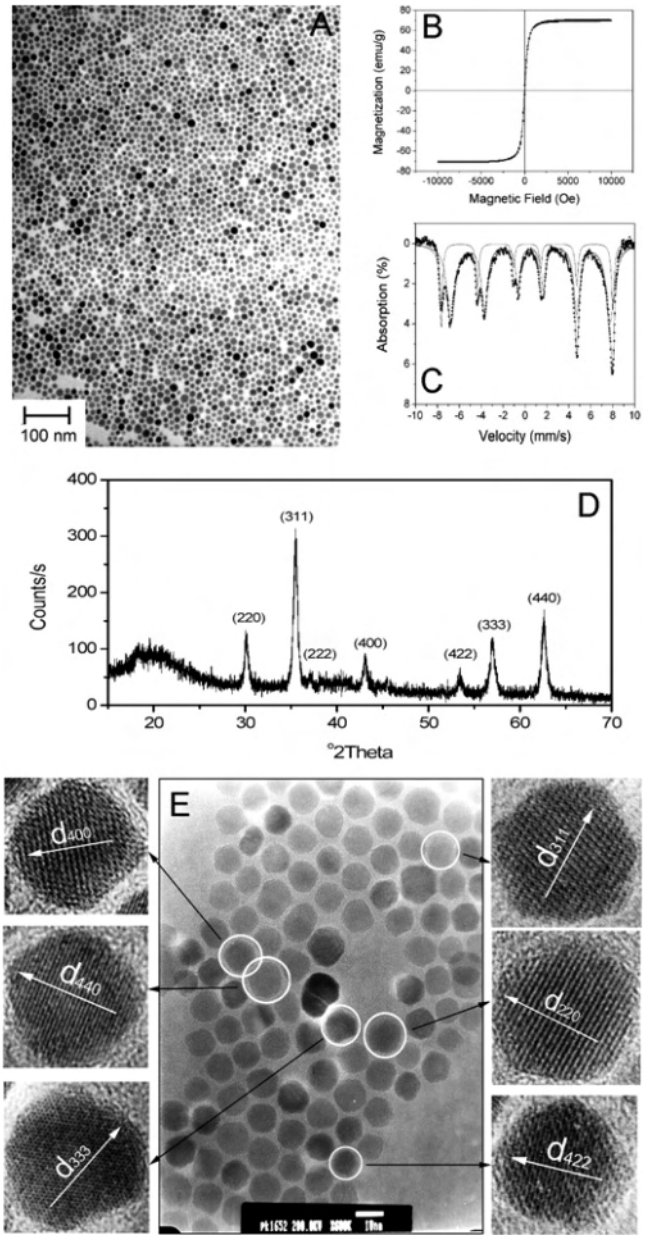

Figure 1. Evolution of shape, size, magnetic property, and crystal structure after annealing of the Fe^{2+}−oleate$_2$ complex at 573 K under 300 mTorr for 2 h. (A) TEM image of a drop of Fe_3O_4 nanocrystals/hexane solution. (B) Magnetization versus applied field at 300 K for Fe_3O_4 nanocrystals using VSM. (C) ^{57}Fe Mössbauer spectrum of synthesized Fe_3O_4 nanocrystals. (D) X-ray diffraction pattern of synthesized Fe_3O_4 nanocrystals. (E) High-resolution TEM characterizations of Fe_3O_4 nanocrystals.

images and collected statistics over 150 particles in part A of Figure 1. A monolayer of nanoparticle was observed without any multilayer. Part A of Figure 1 shows an example of an extended area where particles are packed in a highly organized manner, exhibiting a remarkable degree of long-range order. Nearly monodisperse nanoparticles are arranged in a 2D hexagonal closed packed way, demonstrating the uniformity of the particle size. Especially the interparticle spacing is very even. Here, as in most cases, adjacent Fe_3O_4 nanocrystals are separated by a region of approximately 2 nm, which does not exhibit any diffraction contrast. This distance is considerably less than twice the expected oleate length (1.75 nm);[25] interdigitation of the alkyl chains from nearest-neighbor Fe_3O_4 particles can be inferred. The superparamagnetic behavior is documented by the hysteresis loop measured at 300 K as shown in part B of Figure 1. There is almost an immeasurable coercivity (1.7 Oe) at room temperature. This indicates that Fe_3O_4 particles are superparamagnetic and nanosized.[26−28] The saturation magnetization, M_s, is 72.3 emu/g for Fe_3O_4, which is lower than that of bulk magnetite particles (M_{bulk} = 92 emu/g).[29,30] The decrease in M_s is due to the weight of oleate coated on the surface of the Fe_3O_4 nanocrystals and shows the superparamagnetism of magnetite particles, which occurs when the particle size decreases below 30 or 20 nm.[31] From the magnetization curve, it can be seen that the magnetization achieves a saturation of 72.3 emu/g at 2500 Oe. This result differs from that of iron oxide nanocrystals synthesized by the hydrolytic method. They do not need to be saturated by applying a magnetic field of more than 10 000 Oe.[30,31] The result can be explained from the difference in nanocrystals and the size distributions of the iron oxide nanoparticles. Compared with other iron oxide nanoparticles, produced Fe_3O_4 nanoparticles possess not only a more regular spherical shape but also better monodispersity and crystallinity. The Mössbauer spectrum of the Fe_3O_4 nanocrystals is given in part C of Figure 1 at room temperature. The solid line is a computer-fitted Mössbauer spectrum, and the solid circles give the experimental Mössbauer spectrum. The spectrum was convoluted to two sextets that correspond to iron ions in tetrahedral (T_d) A and octahedral (O_h) B sites of magnetite. Fe_3O_4 can be written as $Fe^{3+}(Fe^{2+}\ Fe^{3+})O_4$. A fast electron-transfer process (electron hopping) between Fe^{2+} and Fe^{3+} ions on the O_h B site takes place above 110−120 K. The spectrum shows clearly two hyperfine magnetic splitting, which is clear evidence for magnetite. The XRD pattern of the Fe_3O_4 nanocrystals sample was shown in part D of Figure 1. No impurity peak is observed in the X-ray diffraction pattern. The diffraction peaks are broadened, which is a result of the reduced particle size. The discernible peaks can be indexed to (220), (311), (222), (400), (422), (333), and the (440) planes of a cubic unit cell, which corresponds to that of the magnetite structure (JCPDS card no. 79−0418). Part E Figure 1 shows lattice images of Fe_3O_4 nanoparticles. It is perfectly matched with the result of the XRD study.

Figure 2 shows TEM images of Fe_3O_4 nanocrystals prepared at different annealing times of 1 h (A), 2 h (B), 4 h (C), and 6 h (D). The mean sizes of Fe_3O_4 nanocrystals at 573 K for 1 h and 2 h are 6.5 and 9.6 nm, respectively. Their morphologies are almost spherical. When the annealing time is above 3 h, the size of Fe_3O_4 nanocrystals was

(25) Kaneko, F.; Yamazaki, K.; Kitagawa, K.; Kikyo, T.; Kobayashi, M.; Kitagawa, Y.; Matsuura, Y.; Sato, K.; Suzuki, M. *J. Phys. Chem. B* **1997**, *101*, 1803.
(26) Kim, D. K.; Zhang, Y.; Voit, W.; Rao, K. V.; Muhammed, M. *J. Magn. Magn. Mater.* **2001**, *225*, 30.
(27) Vijayakumar, R.; Koltypin, Y.; Felner, I.; Gedanken, A. *Mater. Sci. Eng., A* **2000**, *286*, 101.
(28) Zaitsev, V. S.; Filimonov, D. S.; Presnyakov, I. A.; Gambino, R. J.; Chu, B. *J. Colloid Interface Sci.* **1999**, *212*, 49.
(29) Sato, T.; Iijima, T.; Inagaki, N. *J. Magn. Magn. Mater.* **1987**, *65*, 252.
(30) Han, D. H.; Wang, J. P.; Luo, H. L. *J. Magn. Magn. Mater.* **1994**, *136*, 176.
(31) Sugimoto, T. *Adv. Colloid Interface Sci.* **1987**, *28*, 65.

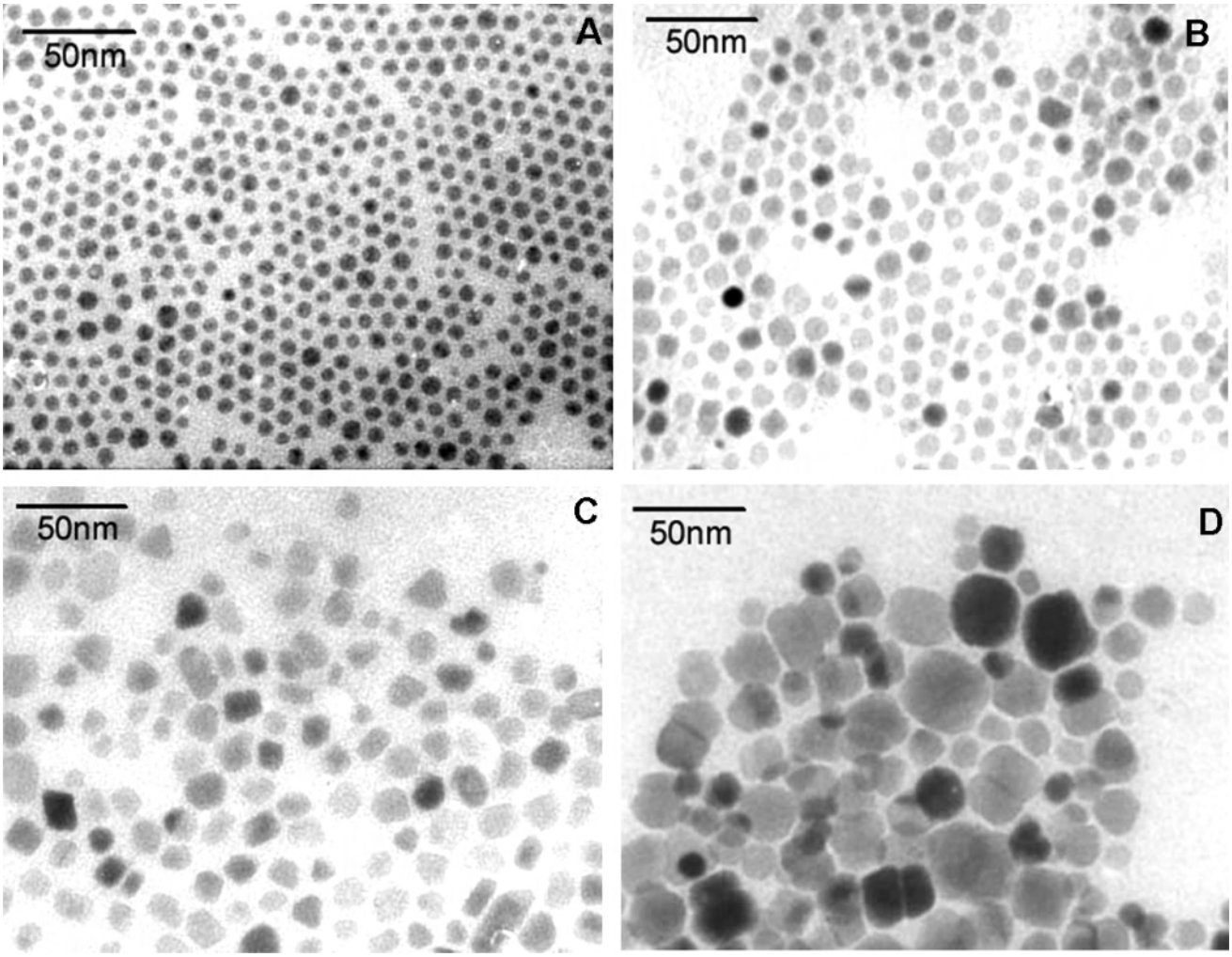

Figure 2. TEM images of Fe_3O_4 nanocrystals. Each of the Fe_3O_4 nanocrystals was prepared at different annealing times (A, 1 h; B, 2 h; C, 4 h; and D, 6 h).

increased, and the shape was changed into shapelessness. These results suggest that the average size of nanocrystals synthesized by thermal decomposition increased over optimized reaction time and also morphology changed. In general, particle size increases with increasing reaction time, as more material adds to particle surfaces, and with increasing temperature, as the rate of addition of materials to the existing nuclei increases. The distribution kinetics approach with single monomer addition and dissociation is reversible and is generally applicable to growth, dissolution, or ripening phenomena known as Ostwald ripening, in which the high surface energy of the smaller particles promotes their dissolution, whereas material is redeposited on the larger particles.[32]

To obtain more detailed information on the thermal decomposition process under different pressure, we carried out a thermalgravimetry analysis connected with a vacuum system. The iron−oleate complex under 300 mTorr started to thermally decompose from 410 K and showed a maximal rate of weight loss at 573 K, which is similar to solution-phase synthesis.[33] TGA/DTG patterns revealed that the loss of 10.54% in the range of 428−524 K is due to the removal of physically adsorbed oleic acid, either free or weakly bound to Fe^{2+} ions at the first DTG peak; then the loss of 26.97% (539−597 K) is owing to the oleate at the surface of nanoparticles, and the residual weight of 62.46% should be that of oleate-capped Fe_3O_4 nanoparticles. These results can explain that the yield between $[Fe]_{decomposed}/[Fe]_{complex}$ is 100%. As we changed the pressure from 300 to 500 mTorr, the decomposition temperature of the iron−oleate complex increased almost 7 K, and no difference was observed between the shapes of the TGA/DTG curves (Supporting Information, Figure S1).

As shown in Figure 3, low-resolution TEM images (A, B) and a high-resolution image (C) of polymorphologies of Fe_3O_4 nanocrystals were produced at 593 K after sealing under 500 mTorr as well as lattice images of spherical-shaped (D), regular triangular-shaped (E), short rod-shaped (F), diamond-shaped (G), and long rod-shaped (H) Fe_3O_4 nanocrystals. It indicated that various shaped nanocrystals were highly crystallized as a Fe_3O_4 crystal structure. From TGA and TEM results, we suggest that the decomposition temperature is increasing and decreasing the velocity of mono-

(32) Zhang, X. L.; Kang, Y. S. *Inorg. Chem.* **2006**, *45*, 4186.

(33) Park, J.; An, K.; Hwang, Y.; Park, J.-G.; Noh, H.-J.; Kim, J.-Y.; Park, J.-H.; Hwang, N.-M.; Hyeon, T. *Nat. Mater.* **2004**, *3*, 891.

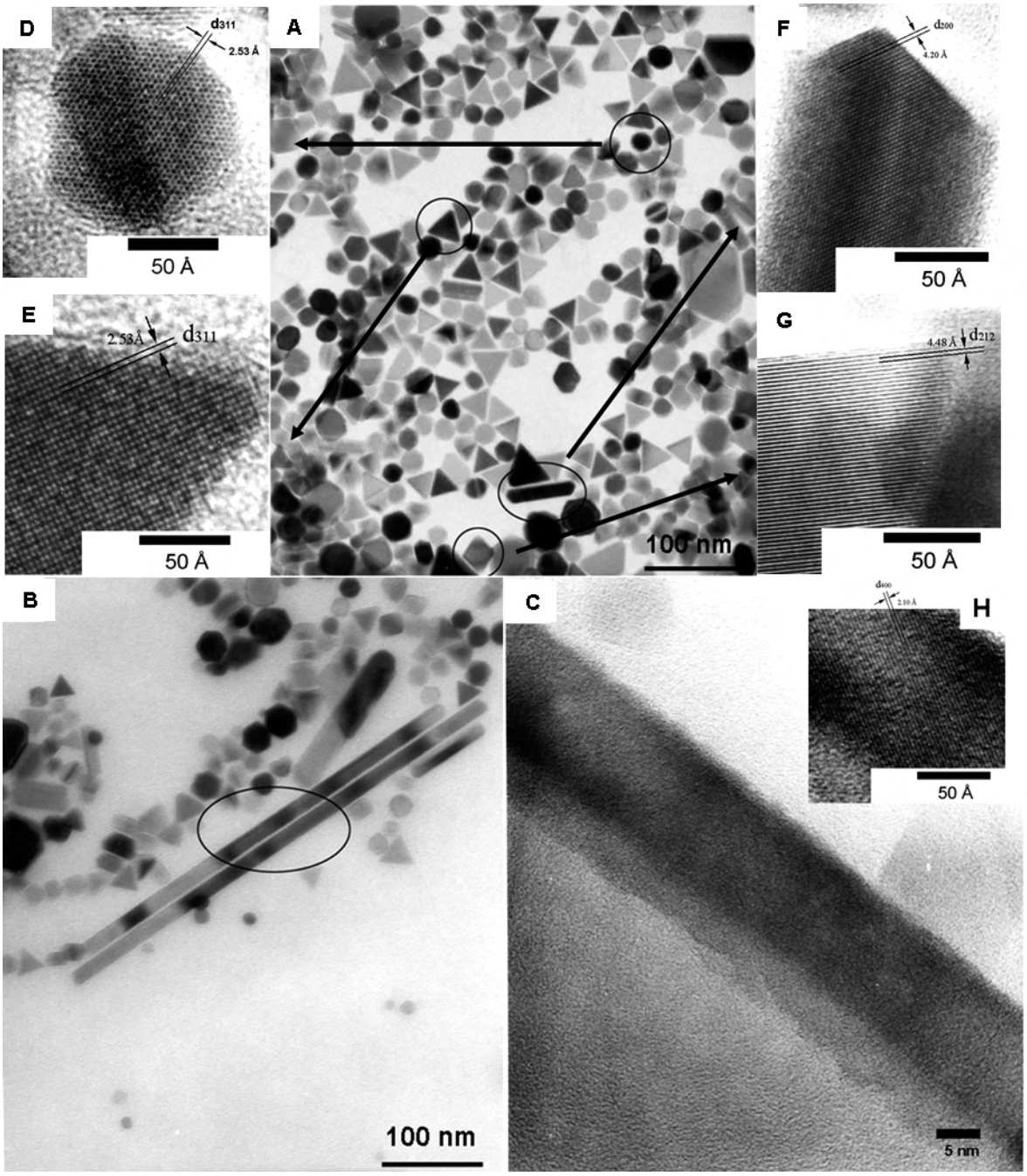

Figure 3. TEM images show a various particle shape of Fe_3O_4 nanocrystals produced at 573 K after sealing under 500 mTorr. (A, B) TEM Images and (C) high-resolution image of differently shaped Fe_3O_4 nanocrystals. (D) Spherical-shaped, (E) regular triangular-shaped, (F) short rod-shaped, (G) diamond-shaped, and (H) long rod-shaped Fe_3O_4 nanocrystals. These lattice images revealed the highly crystalline nature of the nanocrystals.

mer addition to the particle surface, which nucleates nanocrystals as pressure increases in the pyrex tube. It occurs that the nucleation of iron nanocrystals was slow. Generally, a faster nucleation leads to more particles of smaller size, whereas a slower nucleation gives fewer particles of larger size. Particles consist with more than one crystal structure or polymorphs. Polymorphs with different shapes have different surface properties, which influences the growth rate of crystal faces and shape the crystal habit.[34]

3.2. Silver Nanocrystals. Part A of Figure 4 shows a low-resolution TEM image of silver nanocrystals, which are perfectly spherical. The mean size of the silver nanocrystals is 9.5 nm with a standard deviation of 0.7 nm, which was obtained from enlarged images and collected statistics over 150 particles in part A of Figure 4. Part B of Figure 4 shows the UV−vis spectrum of silver nanocrystals ($\lambda_{max} = 420$ nm) dispersed in hexane. The silver nanocrystals display an optical absorption band peaked at 420 nm (~3 eV), typical of the absorption of metallic silver nanocrystals, as a result of the surface plasmon resonance (SPR). The colloidal

(34) Wang, Y.; Xu, X.; Tian, Z.; Zong, Y.; Cheng, H.; Lin, C. *Chem.—Eur. J.* **2006**, *12*, 2542.

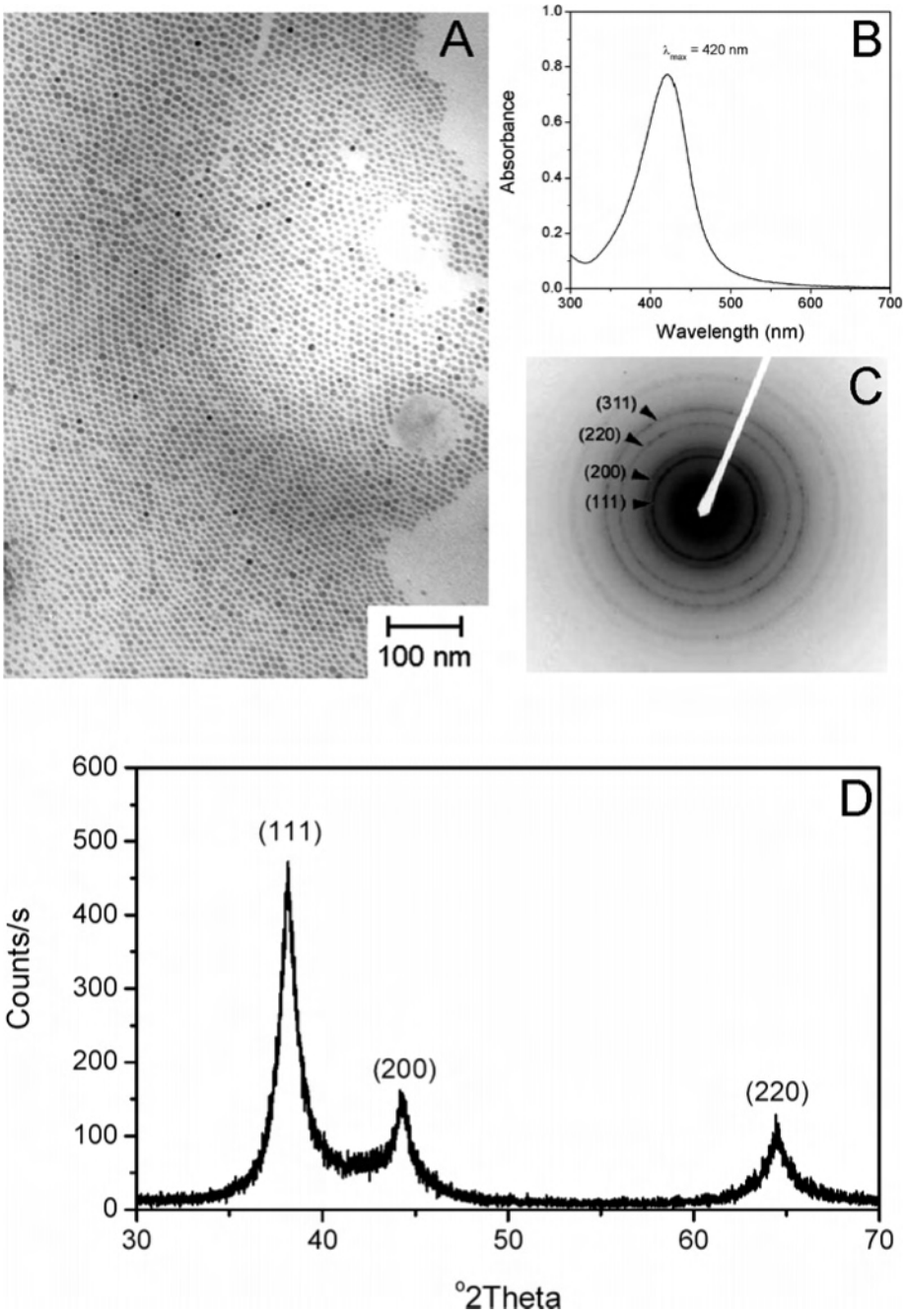

Figure 4. Analysis of silver nanoparticles synthesized by annealing of the Ag^{+1}−oleate complex at 573 K under 300 mTorr for 2 h. (A) Low-resolution TEM image of monodispersed silver nanocrystals was identified. (B) UV−vis spectrum of silver nanocrystals synthesized at 563 K (λ_{max} = 420 nm) dispersed in hexane solution. (C) The selected area diffraction pattern of silver nanocrystals synthesized by solventless thermolysis. (D) XRD pattern of synthesized nanocrystals.

suspensions of our silver particles gave a bright yellow-greenish color due to the intense bands around the excitation of SPR. Although the conduction and valence bands of semiconductors are separated by a well-defined band gap, metal nanocrystals have close-lying bands and electrons move quite freely. The free electrons give rise to a surface plasmon absorption band in metal clusters, which depends on both the cluster size and chemical surroundings. This absorption band is a little blue-shifted compared with the plasmon absorption band of silver colloids prepared by the citrate reduction method (λ_{max} = 434 nm). This is caused because the silver nanocrystals have a narrower size distribution and smaller diameter than silver nanocrystals prepared by the citrate reduction method. Part C of Figure 4 shows that the electron diffraction pattern exhibits a silver crystal structure. The diffraction rings can be indexed to (111), (200), (220), and (311) planes of a silver nanocrystal. Part D of Figure 4 illustrates the XRD pattern of the annealed Ag^{+1}−oleate complex at 563 K under 300 mTorr. The signature of silver is observed. Peaks are broadened due to the nanocrystal nature of silver (JCPDS card no. 04−0783). Three peaks at three values of 38.2, 44.5, and 64.5° correspond to (111), (200), and (220) planes of silver, respectively. No impurity peak is observed in the X-ray diffraction pattern. The

formation of a silver nanocrystal by thermal decomposition was investigated by TGA (Supporting information, Figure S2).

Conclusion

In conclusion, an interesting experimental finding related to a very simple synthetic method of metal nanocrystals and their morphological control has been observed. This work has shown the following results: (1) monodispersed metal nanoparticles were prepared by metal−oleate thermal decomposition without any solvent. (2) Different shaped metal nanocrystals were prepared by annealing time and vacuum pressure and each have a highly crystalline structure. This synthetic procedure developed in the present study offers several very important advantages over the previously reported method[33] for the synthesis of monodispersed nanocrystals. First, this process is easily scaled up for industrial purposes in a single reaction. When the reactor volume is set large, several kilograms of monodispersed nanocrystal can be readily obtained. Second, the synthetic process is environmentally friendly and economical because it uses nontoxic and inexpensive reagents and solvents. Third, the synthetic method is a generalized process that can be easily extended to other metals and to alloys of two or more metal nanocrystals.

Acknowledgment. The author would like to thank to Dr. S. B. Kang at the Cooperative Laboratory Center, Pukyong National University, for assisting in the TEM measurement and Dr. H. J. Ryoo for conducting XRD measurements of our samples. Financial support is from the Program for the Training of Graduate Students in Regional Innovation, which was conducted by the Ministry of Commerce, Industry and Energy of the Korean Government, Brain Korea 21 project in 2007 and Nano R&D Program (Korea Science & Engineering Foundation, Grant 2007-02628). D.K.L. is supported by the Korea Research Foundation Grant funded by the Korean Government (MOEHRD, KRF-2005-214-C00206).

Supporting Information Available: TGA results of Fe and Ag−oleate complex (PDF). This material is available free of charge via the Internet at http://pubs.acs.org.

IC701570Z